of estrogenic agents on reproduction may be misleading and could mask our appreciation of how global exposure to estrogenic xenobiotics threatens wildlife, domestic animals, and our own species.

References and Notes

1. S. Jobling, T. Reynolds, R. White, M. G. Parker, J. P. Sumpter, *Environ. Health Perspect.* **103**, 582 (1995); F. S. vom Saal *et al.*, *Toxicol. Ind. Health* **14**, 239 (1998).
2. C. Sonnenschein and A. M. Soto, *J. Steroid Biochem. Mol. Biol.* **65**, 143 (1998).
3. D. L. Davis, N. T. Telang, M. P. Osborne, H. L. Bradlow, *Environ. Health Perspect.* **105** (suppl. 3), 571 (1997); L. J. Paulozzi, J. D. Erickson, R. J. Jackson, *Pediatrics* **100**, 831 (1997); A. Shibata, J. Ma, A. S. Whittemore, *J. Natl. Cancer Inst.* **90**, 1230 (1998); S. H. Swan and E. P. Elkin, *Bioessays* **21**, 614 (1999).
4. A. M. Soto and C. Sonnenschein, *Comments Toxicol.* **5**, 329 (1996); J. Blanco-Rodriguez and C. Martinez-Garcia, *J. Reprod. Fertil.* **110**, 61 (1997).
5. G. E. Bradford, *Genetics* **58**, 283 (1968); R. B. Land and D. S. Falconer, *Genet. Res.* **13**, 25 (1969); V. D. Toelle, B. H. Johnson, O. W. Robison, *J. Anim. Sci.* **59**, 967 (1984).
6. G. E. Bradford, J. L. Spearow, J. P. Hanrahan, in *Reproduction in Domestic Animals*, P. T. Cupps, Ed. (Academic Press, New York, 1991), pp. 605–636.
7. J. L. Spearow, in *Polycystic Ovary Syndrome*, R. J. Chang, Ed. (Springer-Verlag, New York, 1996), pp. 1–20.
8. ———, *J. Reprod. Fertil.* **82**, 787 (1988); J. L. Spearow and M. Barkley, *Biol. Reprod.* **61**, 851 (1999).
9. R. B. Land, *Nature* **241**, 208 (1973).
10. J. L. Spearow, J. Turgai, F. C. Mao, P. Smith, B. Trost, *J. Anim. Sci.* **65** (suppl. 1), 399 (1987).
11. S. Erickson *et al.*, *Biol. Reprod.* **52** (suppl. 1), 70 (1995).
12. G. E. Bradford, *Genetics* **61**, 905 (1969).
13. J. L. Spearow and G. E. Bradford, *J. Reprod. Fertil.* **69**, 529 (1983).
14. Mice were maintained at 20° to 23°C on a 14 hours light/10 hours dark photoperiod and received Agway 2000 rodent chow (18% protein, 4% fiber, and 9% fat) ad libitum. At 22 to 23 days of age, mice were anesthetized with Avertin (0.012 ml per gram of body weight) and implanted subcutaneously with silastic implants (5 to 10 mm long, 1.5 mm inner diameter, 3.5 mm outer diameter) containing 0, 2.5, 10, 20, or 40 μg of ethanol-dissolved E_2 in Silgard184. At 43 days of age, mice were killed, testis weight was measured, and testes were fixed in phosphate-buffered formalin [3.7% formaldehyde and 75 mM $NaPO_4$ (pH 7.3)], embedded in paraffin, sectioned at 4 μm, and stained with hematoxylin and eosin (H&E). Experiments were conduced in accordance with Association for Assessment and Accreditation of Laboratory Animal Care–approved protocols. Statistical analyses were conducted with one- and two-way analysis of variance with Tukey-Kramer multiple range tests. Initial E_2 release rates averaged 40.25 and 219.5 ng/day from 2.5- and 10-μg E_2 implants, respectively (*23*).
15. H. Inano, K. Suzuki, M. Onoda, K. Wakabayashi, *Carcinogenesis* **17**, 355 (1996).
16. Histological analysis was conducted on phosphate-buffered, formalin-fixed, paraffin-embedded, H&E- and periodic acid–Schiff–stained testicular sections. H&E-stained histological sections from an average of six mice per strain × E_2 dose treatment group were coded and evaluated "blindly" to determine spermatogenic index and the percentage of seminiferous tubules showing sperm maturation to the elongated spermatid stage of development. Germ cells of all CD-1 mice treated with up to 20-μg E_2 implants and seven out of eight mice treated with 40-μg E_2 implants progressed through spermatogenesis as shown by the abundance of normally maturing elongated spermatids and the presence of mature spermatids undergoing spermiation (Fig. 2C). All histological indicators of testicular development declined in B6 mice in response to as little as 2.5-μg E_2 implants (Fig. 2E) and were maximally disrupted in response to 10-μg E_2 implants. Treatment of B6 mice with 10-μg E_2 resulted in vacuolized seminiferous epithelium with disorganized germ cells in the majority of tubules (Fig. 2F). Several B6 mice treated with 10-μg E_2 showed even more extreme testicular atrophy (*18*).
17. J. M. Whitsett, P. F. Noden, J. Cherry, A. D. Lawton, *J. Reprod. Fertil.* **72**, 277 (1984).
18. J. L. Spearow *et al.*, data not shown.
19. The possibility that the high resistance of CD-1 males to E_2 was simply due to heterosis seems unlikely because outbred sublines of CN^- and E were not more resistant to endocrine disruption than inbred sublines. Furthermore, all CD-1 males were highly resistant to endocrine disruption.
20. M. Silberberg and R. Silberberg, *Proc. Soc. Exp. Biol. Med.* **78**, 161 (1951); P. J. Claringbold and J. D. Biggers, *J. Endocrinol.* **12**, 9 (1955).
21. J. W. Pollard, *Endocrinology* **140**, 553 (1999); R. J. Roper *et al.*, *ibid.*, p. 556; B. W. Kirkpatrick, A. Mengelt, N. Schulman, I. C. A. Martin, *Mamm. Genome* **9**, 97 (1998); J. L. Spearow *et al.*, *Biol. Reprod.* **61**, 857 (1999).
22. WHO-Contraceptive-Task-Force, *Lancet* **336**, 955 (1990); H. Behre *et al.*, *J. Clin. Endocrinol. Metab.* **80**, 2394 (1995).
23. C. Munro and G. Stabenfeldt, *J. Endocrinol.* **101**, 41 (1984).

1 April 1999; accepted 20 July 1999

Rapid Infection of Oral Mucosal-Associated Lymphoid Tissue with Simian Immunodeficiency Virus

Christiane Stahl-Hennig,[1] Ralph M. Steinman,[2] Klara Tenner-Racz,[3] Melissa Pope,[2] Nicole Stolte,[1] Kerstin Mätz-Rensing,[1] Gudrun Grobschupff,[3] Birgit Raschdorff,[3] Gerhard Hunsmann,[1] Paul Racz[3]

The early events during infection with an immunodeficiency virus were followed by application of pathogenic simian immunodeficiency virus atraumatically to the tonsils of macaques. Analyses by virologic assays and in situ hybridization revealed that the infection started locally in the tonsils, a mucosal-associated lymphoid organ, and quickly spread to other lymphoid tissues. At day 3, there were few infected cells, but then the number increased rapidly, reaching a high plateau between days 4 and 7. The infection was not detected in the dendritic cell–rich squamous epithelium to which the virus was applied; instead, it was primarily in $CD4^+$ tonsillar T cells, close to the specialized antigen-transporting epithelium of the tonsillar crypts. Transport of the virus and immune-activating stimuli across this epithelium would allow mucosal lymphoid tissue to function in the atraumatic transmission of immunodeficiency viruses.

Virologic and immunologic events during the initial period of human immunodeficiency virus–type 1 (HIV-1) infection have important consequences for vaccine design and the eventual clinical course (*1, 2*). The level of virus or set-point that develops after acute infection correlates with the rapidity with which the disease develops and acquired immunodeficiency syndrome (AIDS) appears (*3*). To observe early events during the transmission of an immunodeficiency virus, and to establish the role of mucosal-associated lymphoid tissue (MALT) at body surfaces, we applied simian immunodeficiency virus (SIV) directly to the surface of the tonsils in macaques. We then followed the kinetics of virus multiplication and spread within and from a single lymphoid organ.

[1]German Primate Center, 37077 Göttingen, Germany. [2]Laboratory for Cellular Physiology and Immunology, Rockefeller University, New York, NY 10021–6399, USA. [3]Bernhard Nocht Institute for Tropical Medicine, 20359 Hamburg, Germany.

This experimental design also provided information on the relative roles of two types of tissue in the early replication of virus. One tissue is the stratified squamous epithelium that overlies the tonsils. It is rich in dendritic cells (DCs) and comparable to the lining of the vagina and anus, tissues that are implicated in genital transmission of HIV-1. The other tissue is the lymphoid component of the tonsil and is comparable to MALT found in the rectum. A critical feature of MALT is a specialized epithelial covering that contacts the underlying lymphoid tissue and contains membranous or microfold "M" cells. Antigens, including virions (*4, 5*), are transported through M cells without the need for trauma or inflammation (*6–9*). Beneath the epithelium lie numerous DCs (*10, 11*), which are important for capturing antigens and initiating T cell–mediated immunity (*12*). There are many observations in tissue culture indicating that DCs contribute to the capture of HIV-1 and SIV and subsequent transmission to T cells (*13–17*).

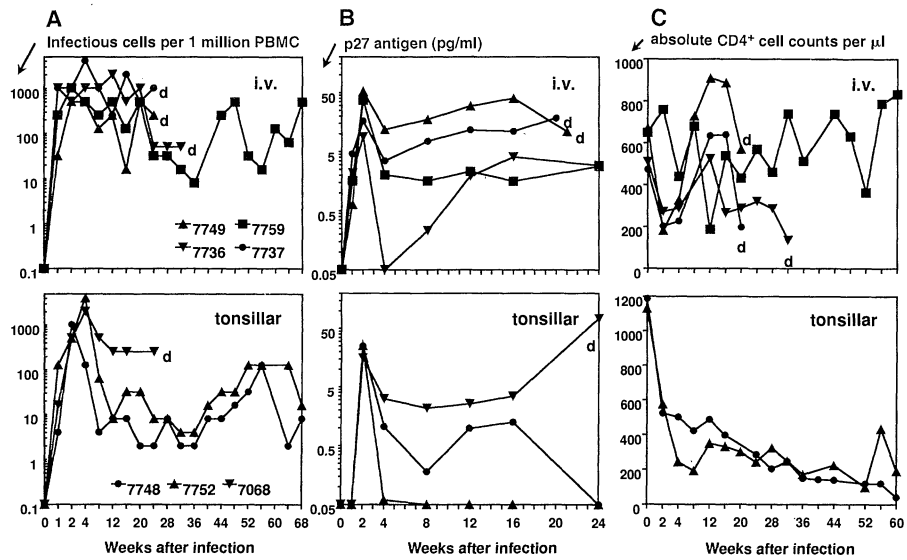

Fig. 1. Markers of infection over time in rhesus macaques after intravenous (iv, upper panels) or tonsillar inoculation (lower panels) with SIVmac251. (**A**) Cell-associated viral load in PBMCs was determined by a limiting dilution coculture technique and the endpoint calculated. Viral loads are expressed as the number of infectious units per 10^6 PBMCs. (**B**) Levels of plasma antigenemia, measured as picograms of p27 capsid antigen per millilter. (**C**) Absolute $CD4^+$ T cells in blood (but not determined in animal 7068) after FACS analysis for CD4 in a lymphocyte gate. The four-digit numbers are macaque designations; d indicates an AIDS-related death.

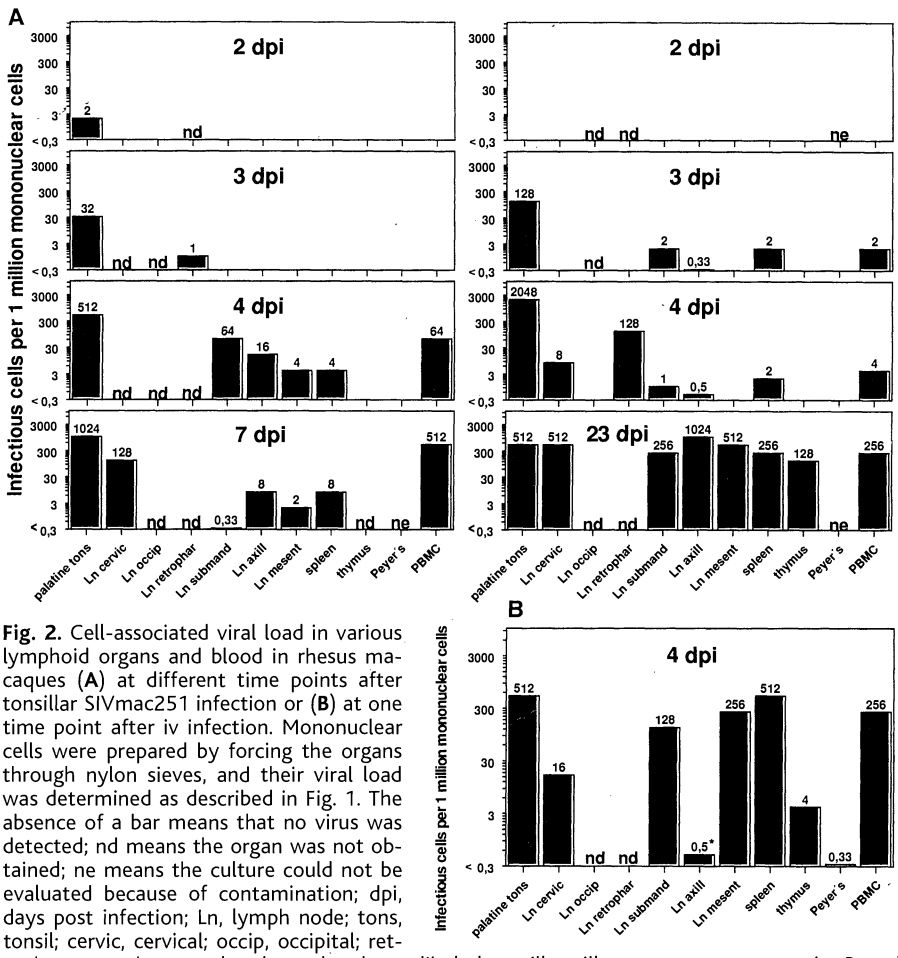

Fig. 2. Cell-associated viral load in various lymphoid organs and blood in rhesus macaques (**A**) at different time points after tonsillar SIVmac251 infection or (**B**) at one time point after iv infection. Mononuclear cells were prepared by forcing the organs through nylon sieves, and their viral load was determined as described in Fig. 1. The absence of a bar means that no virus was detected; nd means the organ was not obtained; ne means the culture could not be evaluated because of contamination; dpi, days post infection; Ln, lymph node; tons, tonsil; cervic, cervical; occip, occipital; retrophar, retropharyngeal; submand, submandibularly; axill, axillary; mesent, mesenteric; Peyer's, Peyer's patches; PBMC, peripheral blood mononuclear cells. The asterisk in (B) indicates an organ in which the end point was not reached because of poor cell yield.

We first administered pathogenic SIVmac251 to juvenile or adult rhesus monkeys of either sex, by intravenous (iv) and tonsillar routes (*18*). For the latter, 200 to 3000 infectious units were applied directly to the palatine and lingual tonsils. To avoid trauma, we touched the tonsils lightly with a cotton-wool swab soaked with culture medium containing cell-free virus (*19*). Thereafter, the infection was monitored in the blood (Fig. 1). Using limiting dilution assays (*20*), we detected infectious virus in peripheral blood mononuclear cells (PBMCs) of all animals within 1 week, and titres peaked at 3 to 4 weeks (Fig. 1A). SIV levels then fell but persisted for more than a year (Fig. 1A). SIV antigen was detected in the blood of all animals with varying persistence over time (Fig. 1B). SIV-specific antibodies appeared by week 3 after infection in all monkeys (*21*), and the number of $CD4^+$ T cells fell shortly after the acute stage of infection (Fig. 1C).

In the next experiment, two animals each were monitored at days 2, 3, and 4, and one animal at days 7 and 23. At each time point, the animals were euthanized and lymphoid tissues were taken for virology and histology examination. Infectious virus at a very low level was already detectable in the palatine tonsil at day 2 in one of two animals. By day 3, virus was detectable in the tonsil in both

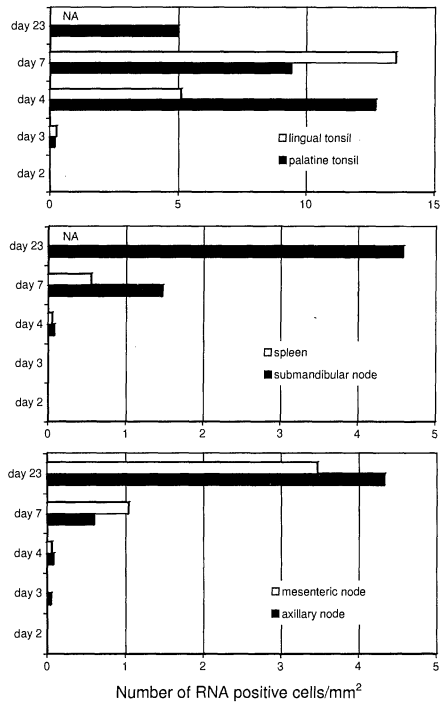

Fig. 3. Summary of the number of infected cells per square millimeter of section, according to in situ hybridization of the indicated lymphoid tissues, for all animals infected by the tonsillar route. The absence of a bar means that no infected cells were seen, for example, at day 2 in tonsils. NA, not available.

animals and reached plateau levels on day 4 and 7 (Fig. 2A). Virus was detected in PBMCs in one of two animals at day 3 and in both at day 4, but the titres of SIV were much less than those seen in the tonsil at day 7 (Fig. 2A). Among the lymphoid tissues we examined, the submandibular and retropharyngeal nodes that drain the tonsil had the most rapid infection (Fig. 2A). By day 3-4, virus had spread to the spleen and distal lymph nodes (mesenteric, axillary), but replication was slow at these time points. By day 23, virus titres in distal lymphoid tissues reached the levels found in tonsils at day 4-7 (Fig. 2A). Therefore, SIV infection was beginning locally in the tonsils and then spreading rapidly to other lymphoid tissues.

We examined the intestine to rule out uptake of swallowed virus into gut MALT. Abundant virus was only found by day 23 by in situ hybridization in the MALT of rectum, duodenum, and small intestine, so it is unlikely that swallowed virus was infecting the monkeys. To verify that the rapid tonsil infection was not due to trauma and entry of virus into the blood, we infected an animal with 2000 $TCID_{50}$ intravenously and examined tissues at day 4. Infection was detected in the tonsil, but its extent was similar to that in spleen and only slightly greater than that in PBMCs and other lymphoid tissues (Fig. 2B). In contrast, application of SIV to the tonsil yielded an infection that was much more intense in tonsil than in spleen or blood (Fig. 2A), indicating that atraumatic application of SIV to the tonsil infects the MALT directly and not via the blood stream.

We measured the rate of infection in the MALT by enumerating the infected cells in

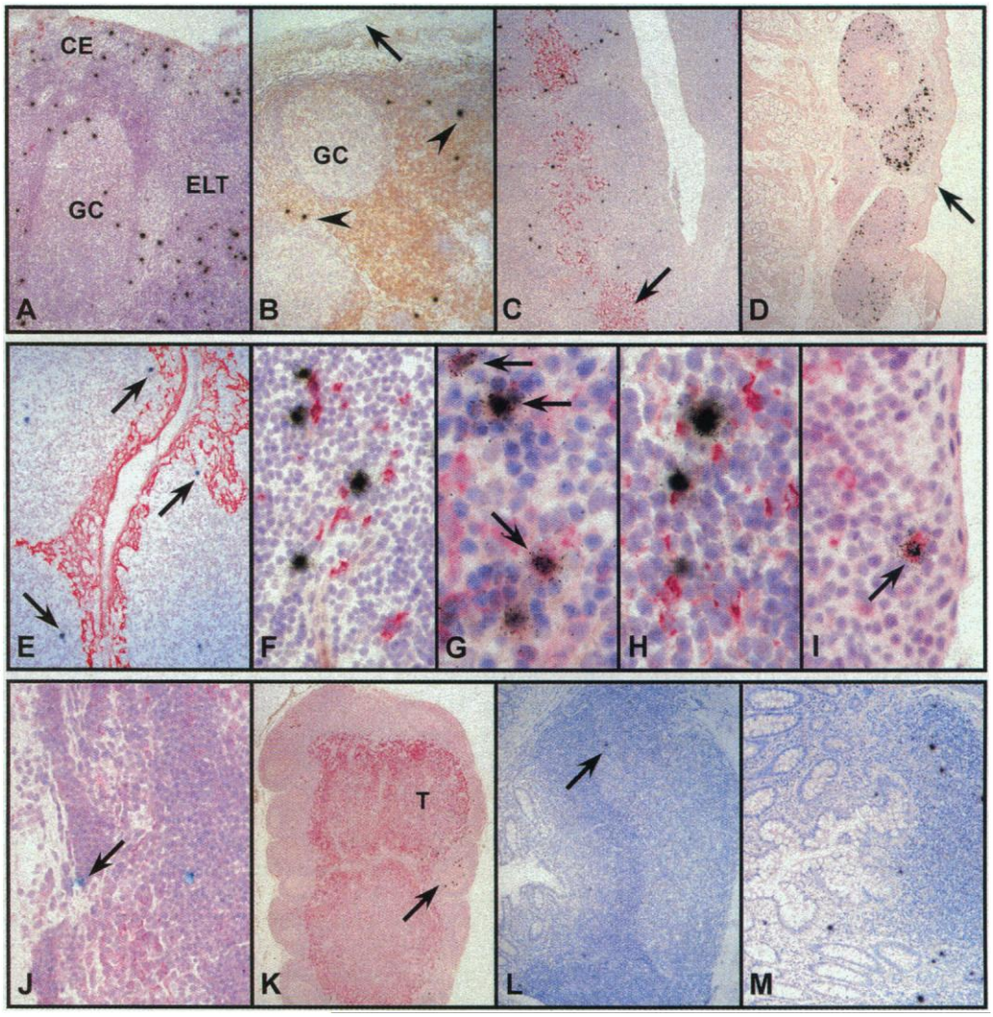

Fig. 4. Localization and identification of infected cells in different tissues by in situ hybridization and immunocytochemistry. (**A**) Rapid productive infection in tonsil, 4 days after atraumatic application of SIVmac. The section is stained in red for CD1a, which marks immature DCs in the crypt epithelium [CE; higher magnification in (F)], and then counterstained with hematoxylin to outline the GC and ELT. Even at this early time point, there are numerous productively infected cells, hybridizing strongly with a radiolabeled antisense SIV probe (black silver grains). Infected cells are found along the CE, in ELT, and less frequently in the GC. (**B**) Same as (A), but the tonsil was examined at day 7 and stained brown for CD3 T cells. Black, productively infected cells are located in regions that are rich in T cells (arrowheads), that is, in the ELT rather than the GC. There are no infected cells in or against the overlying stratified squamous epithelium (arrow). (**C**) Same as (B), but the section was stained in red for p55, a marker of mature DCs that are found in the deeper regions of the tonsil. Most of the black, productively infected cells are located near the CE and ELT, which lack the red network of mature DCs expressing p55 (arrow). (**D**) The sublingual tonsil at day 7 after infection. The squamous epithelium of the tonsil, except for one cell close to the arrow, is not infected, but many underlying tonsillar lymphoid nodules are full of heavily infected cells (black profiles). (**E**) Double labeling of the CE for cytokeratin (red) and SIV RNA (black silver grains) after proteinase K pretreatment. Productively infected cells (for example, at arrows) abut the keratin-positive CE. (**F**) Productively infected cells (black) in the CE are CD1a negative (red). (**G**) Productively infected cells (black) in the extrafollicular T cell areas are $CD4^+$ (red, arrows). There is some loss in intensity of the radiolabel and CD4 images because these lie in different planes of optical focus. (**H**) Productively infected cells (black) lack the CD68 antigen (red) that is abundant in macrophages and found in smaller amounts on DCs. (**I**) High levels of infected, strongly $CD68^+$ (red) macrophages in an animal who died of SIV infection. Because $CD68^+$ infected macrophages were difficult to identify between days 2 and 23 after atraumatic infection of the tonsil, we autopsied an animal that had died from SIV infection. In this animal, CD68+ infected cells were numerous as shown (arrow). (**J**) Infected cells (arrow) in the efferent lymphatic of the tonsil at day 4 after atraumatic application of SIV to the tonsil. Infected cells in a lymphatic could transmit the virus to the adjacent lymph nodes, for example, in the cervical nodes. (**K**) Relatively low levels of infection in distal lymphoid tissue at day 7 after atraumatic application of SIV to the tonsil. In this section of inguinal node, the deep T cell–rich cortex (T) is marked by the network of mature $p55^+$ DCs in red and occupies the entire center of the section. It is surrounded by peripheral cortex with B cell follicles but no red DCs. A single GC has several actively infected cells (arrows). (**L**) Same as (J), but the gut-associated lymphoid tissue is illustrated in a section of the colon. Only a single positive cell (arrow) is found. (**M**) Widespread infection of distal lymphoid tissue in the duodenum 3 weeks after atraumatic application of SIV to the tonsil. Original magnifications: (A and B) ×25, (C and D) ×6.25, (E) ×12.5, (F) ×100, (G and H) ×157.5, (I) ×100, (J) ×50, (K) ×6.25, (L and M) ×25.

sections using in situ hybridization with radiolabeled antisense RNA probes (*22*). Some infected cells were seen at day 3 in palatine and lingual tonsils; however, the number of infected cells then expanded rapidly, peaking between days 4 and 7 (Fig. 3). Small numbers of productively infected cells were observed at day 7 in distal nodes, spleen, and MALT, but only at day 23 were such cells numerous (Fig. 3).

Infected cells were noted in all compartments of the tonsil (except for the stratified surface epithelium), including the lymphocyte-rich lymphoepithelium (LE) of the crypts (containing $CD1a^+$ immature DCs), the germinal centers (GCs) of the B cell follicles, and the outermost extrafollicular lymphoid tissue (ELT) (Fig. 4A). When counted, 86 and 89% of the infected cells were in the ELT at days 4 and 7, respectively, 8% in the LE at both times, and 6 and 3% in GCs. ELT is rich in $CD3^+$ T cells (Fig. 4B), but most infected cells were not in classical deep T cell areas of the ELT, as defined by the presence of mature DCs with the p55 marker (Fig. 4C).

A similar situation was noted in lingual tonsil, which consists of many lymphoid nodules, each connected to the pharynx by an invaginating crypt. The number of infected cells varied from one tonsil nodule to another, but most nodules were infected, and infected cells were numerous especially in p55-negative regions of the ELT (Fig. 4D). In the lingual tonsil at day 7, 74% of infected cells were in ELT, 6% in LE, and 20% in GCs.

We expected that productive infection with SIV would begin in stratified squamous epithelium that constitutes the external covering of the tonsil (Fig. 4B), tongue (Fig. 4D), and buccal cavity (*21*). This epithelium is comparable to the surface of the vagina and anus, and is rich in DCs that can capture and transport immunodeficiency viruses (*13–17*). When we infected the monkeys, we applied SIV directly to the tonsillar squamous epithelium. Breaks in this epithelium also could have provided a conduit for SIV to access susceptible lymphocytes. However, infected cells were not seen beneath the squamous epithelium that directly covered the lymphoid tissue at days 2 to 7 (for example, Fig. 4B), except for one cell in the squamous epithelium covering the tongue on day 7 (arrow, Fig. 4D), but they were abundant along many of the crypts in lingual and palatine tonsils (Figs. 4, A, C, and E). This observation suggests that SIV accessed MALT directly through antigen-transporting crypt epithelium (for example, by means of antigen-transporting M cells) after gentle application to noninflamed tonsils.

To identify the infected cells that hybridized with antisense SIV RNA probes, we double labeled the sections for RNA and different cellular antigens (*23*). The productively infected cells were labeled for CD4 (Fig. 4G) and CD3 (*21*), but not for the immature DC marker CD1a (Fig. 4F) and the macrophage marker CD68 (Fig. 4H). As a positive control for macrophage infection, we studied a monkey who died from SIV-AIDS. This $CD4^+$ T cell–depleted animal had many infected $CD68^+$ tonsillar macrophages (Fig. 4I).

At day 3 and day 4, we also noted productively infected cells in the efferent lymphatics of the palatine tonsil (Fig. 4J). The lymphatics were engorged with lymphocytes ("sinus lymphocytosis") at these early time points, suggesting that productively infected cells can spread to adjacent lymphoid organs via the efferent lymph (*24*).

The systemic spread of infection was also followed. A few productively infected cells were detected in both the follicular and ELT of spleen (*21*), lymph nodes (Fig. 4K), and MALT (Fig. 4L). By day 23, the infection was active in all lymphoid tissues (Fig. 4M), when SIV was trapped on follicular dendritic cells of the GCs as described (*24*).

Ruprecht and colleagues have shown that SIV can be transmitted by the oral route (*24, 25*), a route that is also implicated in HIV-1 transmission (*1, 27*). Our finding that MALT is an explosive site for oral transmission of SIV suggests that oral MALT or Waldeyer's ring is a potential site for HIV-1 transmission during oral sex, parturition, and breast feeding, and by extension, rectal MALT can mediate anogenital transmission. Two other findings of our study were unexpected: (i) infection expands rapidly within MALT, peaking in the space of a few days, and (ii) there is a lack of infection in the stratified squamous epithelium that lines the pharynx and surfaces of the palatine and lingual tonsil (Fig. 4, B and D), even though it is this kind of DC-rich epithelium that is thought to be critical in sexual transmission across the vagina and anus.

The distinguishing feature of MALT is the presence of a specialized overlying epithelium through which antigens can be transported in the absence of any trauma [reviewed in (*6–9*)]. In the gut-associated MALT, the dome of the Peyer's patches and solitary lymphoid nodules are covered by a specialized columnar epithelium in which M cells transport antigens including proteins, small particles, and virions (*4, 5, 7, 9, 28*). In the pharyngeal MALT or tonsils (nasal, palatine, sublingual), there are deep invaginations or crypts lined by a ramifying, keratinized, lymphocyte-rich epithelium with M cells (*29, 30*). M cells could have a second role beyond virion transport, that is, the transport of antigens and inflammatory stimuli that activate DCs and T cells locally. This lymphoepithelium was shown to be an active site for chronic HIV-1 infection (*10, 31*), but it is now evident that this is an efficient area for transmission and acute infection as well (Figs. 2, 3, and 4).

When studied at the single-cell level, the infected cells were almost entirely $CD4^+$ T cells. The infected cells could be double labeled for viral RNA and for CD3 and CD4, but not for the CD1a, p55, and CD68 antigens that are abundant on immature DCs, mature DCs, and macrophages, respectively. However, recent tissue culture studies indicate that DCs can initiate infection, but once begun, activated T cells become the major site for infection (*32*), presumably because T cells have much higher levels of CD4 and CCR5 than do DCs (*33*). Possibly our in situ method would not detect DCs with low levels of viral transcripts.

Our findings, by documenting the rapid development of an infection with immunodeficiency virus within MALT, emphasize new demands for the development of an HIV-1 vaccine. Because viral replication is so robust, reaching a plateau locally in 4 to 7 days and systemically in less than 3 weeks, vaccine-induced immune mechanisms have to be activated very quickly after mucosal transmission.

References and Notes

1. T. Schacker, A. C. Collier, J. Hughes, T. Shea, L. Corey, *Ann. Intern. Med.* **125**, 257 (1996).
2. A. S. Fauci, *Nature* **384**, 529 (1996).
3. J. W. Mellors *et al.*, *Ann. Intern. Med.* **122**, 573 (1995).
4. H. M. Amerongen *et al.*, *J. AIDS* **4**, 760 (1991).
5. J. E. Wolf *et al.*, *Science* **212**, 471 (1981).
6. M. R. Neutra, E. Pringault, J.-P. Kraehenbuhl, *Annu. Rev. Immunol.* **14**, 275 (1996).
7. A. Frey *et al.*, *J. Exp. Med.* **184**, 1045 (1996).
8. M. R. Neutra, A. Frey, J.-P. Kraehenbuh, *Cell* **86**, 345 (1996).
9. R. L. Owen and T. H. Ermak, *Springer Semin. Immunopathol.* **12**, 139 (1990).
10. S. S. Frankel *et al.*, *Science* **272**, 115 (1996).
11. B. L. Kelsall and W. Strober, *J. Exp. Med.* **183**, 237 (1996).
12. J. Banchereau and R. M. Steinman, *Nature* **392**, 245 (1998).
13. M. Pope *et al.*, *Cell* **78**, 389 (1994).
14. M. Pope, S. Gezelter, N. Gallo, L. Hoffman, R. M. Steinman, *J. Exp. Med.* **182**, 2045 (1995).
15. A. Granelli-Piperno, E. Delgado, V. Finkel, W. Paxton, R. M. Steinman, *J. Virol.* **72**, 2733 (1998).
16. M. Pope, D. Elmore, D. Ho, P. Marx, *AIDS Res. Hum. Retrovir.* **13**, 819 (1997).
17. R. Ignatius, F. Isdell, U. O'Doherty, M. Pope, *J. Med. Primatol.* **27**, 121 (1998).
18. Spleen cells from the original rhesus monkey 251 had been cocultivated with primary rhesus monkey PBMCs. For the preparation of our virus stock, supernatant from that culture was transferred to fresh PBMCs. This stock has an in vitro titre of $10^{4.7}$ median tissue culture infectious dose ($TCID_{50}$) per milliliter when titrated in the human T cell line C81-66. In vivo titration of this stock in rhesus monkeys by the iv route yielded $10^{6.4}$ median monkey infectious doses (MID_{50}); by the rectal route $10^{2.3}$ MID_{50}; and by the vaginal route $10^{1.8}$ MID_{50} [O. Neildez *et al.*, *Virology* **243**, 12 (1998)].
19. We studied juvenile or young adult rhesus monkeys (*Macaca mulatta*) of Indian origin, bred at the German Primate Center or imported from the United States (Laboratory Animal Breeders and Services, Yemassee, NC). Animal care was in accordance with guidelines of the German Primate Center. Monkeys were of either sex, had a body weight of 3.5 to 5 kg and were seronegative for simian T cell lymphoma virus–type 1, D-type virus, and SIV. Animals were housed in single cages

and monitored as described (*34*). All manipulations (virus inoculation, physical exam, and venapuncture) were performed under ketamine sedation. To compensate for increased salivation during sedation, which would enable an accelerated flux of applied virus to the gastrointestinal tract, we injected intraveneously an anti–cholinergic glycopyrroniumbromide just before virus inoculation. For atraumatic exposure of the palatine and lingual tonsils, a cotton-wool swab was saturated with phosphate-buffered saline, squeezed out, and then saturated with an undiluted or 1:10 diluted cell-free virus suspension. Thereafter, these tonsillar regions were repeatedly touched lightly in three 5-min intervals with freshly saturated swabs, finally applying a total volume of ~50 to 80 μl of virus suspension. This applied amount of virus was calculated by weighing the swabs after use and corresponded to ~2000 to 3000 $TCID_{50}$ with undiluted virus (which corresponds to amounts used in many studies of urethral, rectal, and vaginal transmission) and ~200 to 300 $TCID_{50}$ with the diluted virus. At the time of inoculation, no obvious lesions or gingivitis were observed in the oral cavity of any of the animals used. To monitor long-term infection by this route, we followed three macaques, two receiving undiluted virus and one 1:10 diluted virus, for a longer period of time. To determine the site of virus entry and virus spread, we euthanisized another eight monkeys in the acute phase after tonsillar exposure, two each on days 2, 3, and 4 and one each on days 7 and 23 after inoculation. Tonsillar infection was compared with the iv route by infecting other animals intravenously with a similar dose of 2000 $TCID_{50}$ of the same virus stock and monitoring them with virologic assays for several weeks and by histology in one animal on day 4. At necropsy lymphoid and nonlymphoid organs were sampled from various body locations for virus isolation, histology, immunohistochemistry, and in situ hybridization.

20. Cell-associated viral loads were determined by limiting dilution coculture with mononuclear cells from blood and lymphoid organs (*35*). PBMCs were separated from whole citrated blood by Ficoll density gradient centrifugation. To prepare mononuclear cells from lymphoid organs (tonsils, lymph nodes from different regions, spleen, thymus, and Peyer's patches), we forced the respective tissues through commercial nylon sieves (100-μm mesh, Falcon) and processed them like PBMCs except for the density gradient centrifugation. This centrifugation step was only necessary for spleen cells because of the red blood cell contamination. After separation of mononuclear cells, they were simultaneously cocultivated in declining concentrations with human C81-66 T cells as indicators (*35*). Cultures were monitored for syncytia formation, and intracellular antigen was visualized by an immunoperoxidase assay (*36*), with the modification that the T cells were adhered to concanavalin A–coated microtitre plates instead of poly-L-lysine–coated plates. All treated cells were scored under a light microscope, with infected cells being identified by a deep red-brown cytoplasmic staining. The endpoint of the viral load was calculated as described (*35, 37*). Heat-inactivated whole SIV lysate was used in optimal concentrations to coat 96-well microtiter plates to measure serum anti-SIV antibody responses as described (*36*). Antigenemia was measured by a commercial HIV-1/HIV-2 antigen test (Innogenetics, Zwijndrecht, Belgium). To determine the absolute $CD4^+$ T cell counts in blood, we stained PBMCs with phycoerythrin-conjugated antibody to CD4 (OKT4, Ortho Diagnostics Systems) and analyzed them on an EPICS XL flow cytometer (Coulter) with gating on lymphocytes. $CD4^+$ T cell numbers were calculated by multiplying white cell count times lymphocyte percentage in a blood smear times $CD4^+$ T cell percentage by fluorescence-activated cell sorting (FACS).
21. C. Stahl-Hennig et al., data not shown.
22. The 5-μm-thick paraffin or cryostat sections were placed on slides coated with 3-amino-propyl-triethosilane. Four sections from each tissue per time point were hybridized with an ^{35}S-labeled, single-stranded, antisense RNA probe of SIVmac239 (Lofstrand Labs, Gaithersburg, MD). It was composed of fragments of 1.4 to 2.7 kb in size, which collectively represent ~90% of the SIV genome. As a positive control, cytospin prepartions of SIV-infected PBMCs were hybridized, and as a negative control, a sense-strand probe was used. Dewaxed paraffin sections were boiled in a domestic pressure cooker in citrate buffer pH 6.0 for 5 min, chilled down to room temperature, rinsed in water containing 2% diethyl-pyrocarbonate, and prehybridized for 2 hours at 45°C. The prehybridization mixture consisted of 50% formamide, 0.5 M NaCl, 10 mM tris-HCl at pH 7.4, 1 mM EDTA, 0.02% Ficoll-polyvinylpyrrolidone, and 2 mg of tRNA per milliliter. Prehybridization was followed by incubation with the hybridization mixture (prehybridization mixture, 10% dextran sulfate, and 2×10^6 dpm of probe per milliliter) overnight at 45°C in a moist chamber. After several washings in standard saline citrate (SSC), the sections were digested with ribonuclease at 37°C for 40 min, washed again in 2× SSC, dehydrated, and dipped in Kodak NTB-2 emulsion. Exposure at 4°C was for 2 to 3 days for frozen sections and 7 days for paraffin sections. After development in Kodak D-19, sections were counterstained with hemalaun, mounted, and examined with an Axiophot Zeiss microscope equipped with epiluminescent illumination. Viral RNA–positive cells were counted with a 20× objective, a 3CD color camera, and a PC-based image analysis system (KS400; Kontrol, Esching, Germany). Positive cells had >20 silver grains, corresponding to a sixfold excess over background. Four entire sections were counted for each recorded value to obtain a mean number of infected cells per section and per unit area. The percentage of infected cells was then recorded for the epithelial, germinal center, and extrafollicular lymphoid tissue.
23. Immunolabeling was performed on paraffin-embedded and cryostat sections according to the alkaline phosphatase anti–alkaline phosphatase method. Antibodies included CD68 (Dako, macrophages), CK1 (Dako, cytokeratin), p55 (provided by E. Langhoff, mature DCs), CD1a (Immunotech, immature DCs), CD4 (Leu3a, Becton Dickinson; OKT4, Ortho Diagnostics; and NCL, CD-4 1F6 Novocastra; all together), CD8 (Leu2a, Becton Dickinson, and C8/144B, Dako; together), and polyclonal CD3 (Dako, visualized with the peroxidase anti-peroxidase method). Immunolabeling was performed before in situ hybridization.
24. K. Tenner-Racz *et al.*, *AIDS* **2**, 299 (1988).
25. T. W. Baba *et al.*, *Science* **272**, 1486 (1996).
26. R. M. Ruprecht *et al.*, *AIDS Res. Hum. Retrovir.* **14**, S97 (1998).
27. R. B. Rothenberg, M. Scarlett, C. del Rio, D. Reznik, C. O'Daniels, *AIDS* **12**, 2095 (1998).
28. K. Tenner-Racz, P. Racz, Q. N. Myrvik, J. R. Ockers, R. Geister, *Lab. Investig.* **41**, 106 (1979).
29. B. Winther, D. J. Innes, *Arch. Otholaryngol. Head Neck Surg.* **120**, 144 (1994).
30. P. Brandtzaeg, in *Immunology of the Ear*, J. Bernstein and P. Ogra, Eds. (Raven Press, New York, 1987), p. 63.
31. S. S. Frankel *et al.*, *Am. J. Pathol.* **151**, 89 (1997).
32. A. Granelli-Piperno, V. Finkel, E. Delgado, R. M. Steinman, *Curr. Biol.* **9**, 21 (1998).
33. A. Granelli-Piperno *et al.*, *J. Exp. Med* **184**, 2433 (1996).
34. K. L. Molnar-Kimber *et al.*, *Hum. Gene Ther.* **9**, 2121 (1998).
35. C. Stahl-Hennig *et al.*, *J. Gen. Virol.* **77**, 2969 (1996).
36. S. G. Norley, J. Lower, R. Kurth, *Biologicals* **21**, 251 (1993).
37. C. Stahl-Hennig, *et al.*, *Virology* **186**, 588 (1992).
38. We thank A. Aubertin (Strasbourg, France) for providing an early passage of SIVmac251. The ^{35}S-labeled, single-stranded, antisense RNA probe of SIVmac239 (Lofstrand Labs, Gaithersburg, MD) was obtained in collaboration with S. Gartner (Yale University, New Haven, CT) through the NIH Research Program. Grant support was provided by the NIH (AI 42129 and 40874 to R.M.S., and AI 40877 to M.P.), the German Ministry of Education and Research (BMBF, grant number 01KI-9767/9), the Korber Foundation (Hamburg), and the Fogarty Foundation (RO3TW00792).

16 February 1999; accepted 22 July 1999

Conservatism of Ecological Niches in Evolutionary Time

A. T. Peterson,[1]* J. Soberón,[2] V. Sánchez-Cordero[3]

Theory predicts low niche differentiation between species over evolutionary time scales, but little empirical evidence is available. Reciprocal geographic predictions based on ecological niche models of sister taxon pairs of birds, mammals, and butterflies in southern Mexico indicate niche conservatism over several million years of independent evolution (between putative sister taxon pairs) but little conservatism at the level of families. Niche conservatism over such time scales indicates that speciation takes place in geographic, not ecological, dimensions and that ecological differences evolve later.

Critical characteristics of species' biology, such as physiology, feeding ecology, and reproductive behavior, define their fundamental ecological niches (*1*). In the early 1990s, several theoretical community ecologists independently predicted that fundamental niches of species under natural selection could change, but slowly. Based on diverse models that coupled population and genetic dynamics in heterogeneous environments, niche conservatism was predicted, because rates of adaptation in environments outside of the fundamental niche would often be slower than the extinction process (*2*).

However, little empirical evidence has been assembled to address these theoretical predictions (*3*). One study (*4*) that compared population response surfaces to climatic conditions in two closely related species of beeches (*Fagus* spp.) showed that limiting conditions for the presence of populations were coincident. Another study (*5*) documented conservatism in geographic range size in disjunct Asian and North American

[1]Natural History Museum, The University of Kansas, Lawrence, KS 66045, USA. [2]Instituto de Ecología, Universidad Nacional Autónoma de México, México, D.F. 04510, México. [3]Departamento de Zoología, Instituto de Biología, Universidad Nacional Autónoma de México, México, D.F. 04510, México.

*To whom correspondence should be addressed. E-mail: town@ukans.edu